Baniasadi, Hossein; Chatzikosmidou, Despoina; Kankkunen, Ari; Seppälä, Jukka; Yazdani McCord, Maryam R.

Flexible and conductive nanofiber textiles for leakage-free electro-thermal energy conversion and storage

Published in:
Solar Energy Materials and Solar Cells

DOI:
10.1016/j.solmat.2023.112503

Published: 15/09/2023

Document Version
Publisher's PDF, also known as Version of record

Please cite the original version:
Baniasadi, H., Chatzikosmidou, D., Kankkunen, A., Seppälä, J., & Yazdani McCord, M. R. (2023). Flexible and conductive nanofiber textiles for leakage-free electro-thermal energy conversion and storage. *Solar Energy Materials and Solar Cells*, *260*, Article 112503. https://doi.org/10.1016/j.solmat.2023.112503

Solar Energy Materials & Solar Cells 260 (2023) 112503

Contents lists available at ScienceDirect

Solar Energy Materials and Solar Cells

journal homepage: www.elsevier.com/locate/solmat

Flexible and conductive nanofiber textiles for leakage-free electro-thermal energy conversion and storage

Hossein Baniasadi [a], Despoina Chatzikosmidou [a], Ari Kankkunen [b], Jukka Seppälä [a], Maryam R. Yazdani McCord [b,*]

[a] Polymer Technology, School of Chemical Engineering, Aalto University, Espoo, Finland
[b] Department of Mechanical Engineering, School of Engineering, Aalto University, P.O. Box 14400, 00076, Aalto, Finland

ARTICLE INFO

Keywords:
Phase change fibers
Smart textile
Electrical conductivity
Energy storage
Energy conversion

ABSTRACT

In this contribution, a novel flexible phase change textiles based on decanoic acid (DA) and polyamide 11 (PA11) blends with various DA/PA11 mass ratios, in which PA11 acted as the polymer matrix, and DA behaved as phase change ingredient, were developed *via* electrospinning. Besides, a conductive polypyrrole (PPy) coating was designed *via in-situ* polymerization. Morphological observations carried out by the SEM images demonstrated porous and highly homogeneous morphology with smooth, long, continuous, and free-bead fibers. Furthermore, forming of a uniform PPy layer on the surface was confirmed through the images. As such, conductive textiles with electrical conductivity up to 28.89 ± 1.50 S/m were prepared. Tensile testing showed that the mechanical properties did not change considerably after PPy coating. Moreover, the phase change performance was investigated using DSC analysis, where the melting and crystallization enthalpies were respectively 112.77 J/g and 110.21 J/g in the textile with the highest DA loading, i.e., 70 wt%. More notably, the phase-change enthalpies did not change considerably after 100 DSC thermal cycles. Finally, significant electro- and photo-heat storage and conversion were observed for the conductive PCM textiles. Thus, this work introduced new flexible smart textiles with significant potential in wearable and protective systems.

1. Introduction

Nowadays, smart materials with intrinsic functionality in storing latent heat and regulating temperature, known as phase change materials (PCMs), have received significant attention, both scientifically and industrially. They can be found in both organic and inorganic materials as solid-solid, solid-liquid, solid-gas, and liquid-gas systems [1–3]. In the last few years, organic solid-liquid PCMs, like paraffin wax, fatty acids, polyols, and polymers, have received more attention in heat storage and thermal management applications. Examples include solar energy storing systems, air conditioning systems, heat sinks in electronics, smart thermal buffering clothing, heat biosensors for detecting biological species, and wound dressing for thermal protection of healthy tissues during cryosurgery of tumor cells [4–7]. Furthermore, the ability of PCMs to store/release the heat produced by electricity has also been proved. Thus, they have been widely applied in delay switches, off-peak electricity conversion, hybrid electric vehicles, heat sinks of mobile electronic devices, radiant floor heating, and electric-thermal media for clean energy utilization [8]. Nevertheless, their prone to fluidization as well as their considerable volume expansion during phase transition, are two features limiting the PCMs' practical application. Form stabilization is one of the solutions to addressing these drawbacks effectively. As such, considerable efforts have been made to design and fabricate form-stable PCM composites [9,10]. Electrospinning, as a simple and convenient method, offers a straightforward continuous fabrication process for stabilizing PCMs in the network of different polymers without leakage [11,12].

Smart clothing is a variety of responsive products equipped with smart elements, enabling beyond the cover, e.g., self-sensing, self-adaption, self-healing, etc. They have found many applications, including flexible displays, protective garments, wearable sensors, and energy devices [9,13]. Likewise, the integration of PCMs into fibers can offer exciting opportunities for smart clothing in making stronger adaptability of the human body to environmental temperature. Here, flexibility and stretchability are two key features to fulfill the demand for body movement. Most PCMs, on their own, do not provide any

---

* Corresponding author.
E-mail address: roza.yazdani@aalto.fi (M.R. Yazdani McCord).

https://doi.org/10.1016/j.solmat.2023.112503
Received 20 April 2023; Received in revised form 31 July 2023; Accepted 5 August 2023

flexibility required for developing smart clothing. Therefore, efforts have been made to integrate PCMs inside flexible textiles to fabricate smart clothing [9,14–17]. Thanks to its high strength, stiffness, and flexibility, polyamide has been widely used as a fabric. Furthermore, the form stabilization of PCMs with polyamide fibers, mainly polyamide 6, has been practiced for leakage control [16,18–23]. Polyamide 11 (PA11), a castor oil-based polymer, is an attractive polyamide used as an engineering plastic in different industrial fields, from automotive parts to offshore oilfield [24,25]. However, there is no scientific report on the form stabilization of PCMs using PA11 to develop smart textiles or other applications. We hypothesized that the higher melting point of PA11 (∼190 °C) than the room temperature makes it a potential support in developing form-stable phase change textiles.

On the other hand, due to the desired properties and characteristics, such as the large capacitance for latent heat, the appropriate phase change temperature range, the low vapor pressure of melts, little supercooling during phase transitions, and non-toxicity, fatty acids have been extensively studied as a promising type of PCMs [18]. We hypothesized that integrating fatty acids with PA11 fibers can introduce a fully bio-based smart textile for previously mentioned applications. Yet, for some advanced electrical-thermal applications, such as energy conversion and storage systems, the fatty acid/PA11 blend is seriously limited by the inherent low thermal conductivity, electrical insulation, and poor sunlight absorption. Incorporating photo absorbers and conductive materials could efficiently improve the performance of the selected PCM composite in energy conversion and storage systems by reducing the photon/electro-to-thermal conversion gradient. In similar research, metal powders, boron nitride, expanded graphite, carbon nanotubes, and other randomly distributed high thermal conductive fillers have been incorporated into the PCMs-based systems to endow the developed composites with electric-harvesting abilities. Still, conductivity remained low because forming interconnected conductive pathways by directly adding powders or fibers is challenging. More notably, adding excessive conductive fillers caused phase separation and sacrificed the mechanical properties of the composite PCMs [4,8,9]. Conductive polymers, e.g., polypyrrole (PPy), with relatively high electrical conductivity, chemical stability, and ease of synthesis [26], can effectively address these issues. Although PPy's direct blending with electrospinning solution and thereby fabricating conductive textiles might be challenging, *in-situ* polymerization of PPy onto textile fibers could be considered a feasible approach to fabricate conductive fabrics [27–29].

To this aim, we presented an electrospinning-based strategy to develop smart thermal buffering textiles with excellent mechanical properties, high enthalpy, and temperature responsiveness using decanoic acid (DA) as PCM and PA11 as a supporting matrix. Furthermore, we coated a layer of conductive PPy onto the fabricated textiles through *in-situ* polymerization. The PPy layer was formed on the fibers' surface with the idea of developing a strong H-bonding between the polyamide/fatty acid substrate and PPy, resulting in conductivity values up to 28 S/m. The smart energy storage fibers with excellent shape and mechanical stabilities, high heat storage capacities, and electric-to-thermal conversion ability provide new alternative smart textiles in wearable and protective systems.

2. Experimental

2.1. Materials

Polyamide 11 (PA11) FMNO grade was provided by Arkema. Decanoic acid (DA, >98%), pyrrole, and 1,1,1,3,3,3-Hexafluoropropan-2-ol (HFIP, >99.0%) were purchased from Tokyo Chemical Industry. Hydrochloric acid (HCl, 37%) and Iron(III) chloride (anhydrous, powder, ≥99.99% trace metals basis) were obtained from Sigma-Aldrich. Distilled water (DI) was used as a solvent media.

2.2. Phase change textiles fabrication

Fabrics were prepared by an in-house electrospinning device equipped with a high-voltage power supply (0–30 kV), a rotating collector (0–1000 rpm), and a syringe pump. A 12 ml polyethylene syringe with a 20 gauge needle was used for spinning the solutions. First, a 15 wt % of PA11 in HFIP was prepared by dissolving PA11 granules into HFIP at 50 °C. Then, it was used to spin a plain polyamide fabric. The electrospinning parameters, including voltage, needle-to-collector distance, collector speed, and feed rate, were selected as 22 kV, 11 cm, 100 rpm, and 25 μl/min. They were optimized experimentally by monitoring the quality of the fibers. Temperature and humidity were 24 °C and 30%, respectively. Following, PCM fabrics were prepared by adding different concentrations of DA into the PA11 solution. The overall amount of DA and PA11 was fixed at 30 g in 100 ml HFIP solvent (equivalent to 30 wt %), and the mass ratio between DA and PA11 was determined as 15/15, 18/12, and 21/9. They were coded as FAP1, FAP2, and FAP3, respectively.

2.3. In-site polymerization of polypyrrole

The PPy was deposited on the PCM textiles using a chemical polymerization method. The textile was cut to 3 cm × 3 cm and weighted (m_0). It was placed into a beaker under a nitrogen flow and kept inside an ice bath. The spun fabric was impregnated with an identical amount of pyrrole (m_0) added to both sides. The sample was let to soak for 2 h. Then, a calculated amount of $FeCl_3$ dissolved in 1 M HCl was added at once to the pyrrole-wetted textile. The system was kept for 8 h without any stirring. After that, the PPy-coated fabric was removed and washed several times with DI water to remove unreacted monomer and $FeCl_3$, as well as not grafted PPy molecules. The PPy-coated fabrics were then dried at room temperature for 48 h. The PPy-coated PA11, FAP1, FAP2, and FAP3 fabrics were designated as PA-PPy, FAP1-PPy, FAP2-PPy, and FAP3-PPy, respectively.

2.4. Characterization

The chemical structure was analyzed by an FTIR (Fourier transform infrared) with ATR spectrometer model PerkinElmer. The spectra were collected in a wavenumber range from 4000 cm^{-1} to 500^{-1}, with a scan number of 16 and a resolution of 4 cm^{-1}. The morphology of the spun fibers before and after PPy coating was investigated by an SEM (Scanning electron microscopy) device model Zeiss Sigma VP. A thin layer (∼4 nm) of gold-palladium was coated on the surface before the imaging. The diameter of at least 100 fibers was extracted by ImageJ software, averaged, and reported. The surface wettability was characterized by the water contact angle measurement performed on a Theta Flex optical tensiometer. A 10 μl water droplet was placed on the sample's surface, and the contact angle was measured after 10 s and 60 s. The thermal decomposition was monitored by thermogravimetric analysis (TGA) performed on a TA Instruments device model Q500. The sample was heated under a nitrogen atmosphere from 30 °C to 800 °C with a heating rate of 10 °C/min. The electrical conductivity and resistance were measured with a four-point probe (Four-point probe system from Ossila, UK). The sample was cut by 1 cm × 1 cm and its average thickness was measured and entered into the device prior to the measurement. The mechanical properties were measured by a Universal Tester Instron model 5944. A strip-shaped sample (3.2 mm ×55 mm) was cut using a sharp cuter and stretched at a 2 mm/min speed with a load cell of 2 kN. The sample was conditioned for 72 h at a temperature and relative humidity of 24 °C and 55%, respectively. The plain DA, as well as FAP3 and FAP3-PPy fabrics, were kept in the oven at 60 °C for 2 h. Photographs of the samples before and after heating were captured to investigate the probable leakage of DA from the PCM fabrics. The phase change performance was examined by DSC (differential scanning calorimetry) measurement performed on a TA Instruments model Discovery

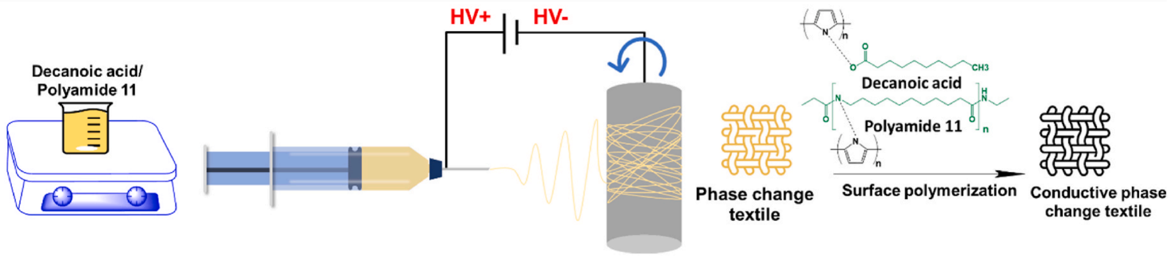

Fig. 1. Schematic representation of the conductive PCM textiles fabrication.

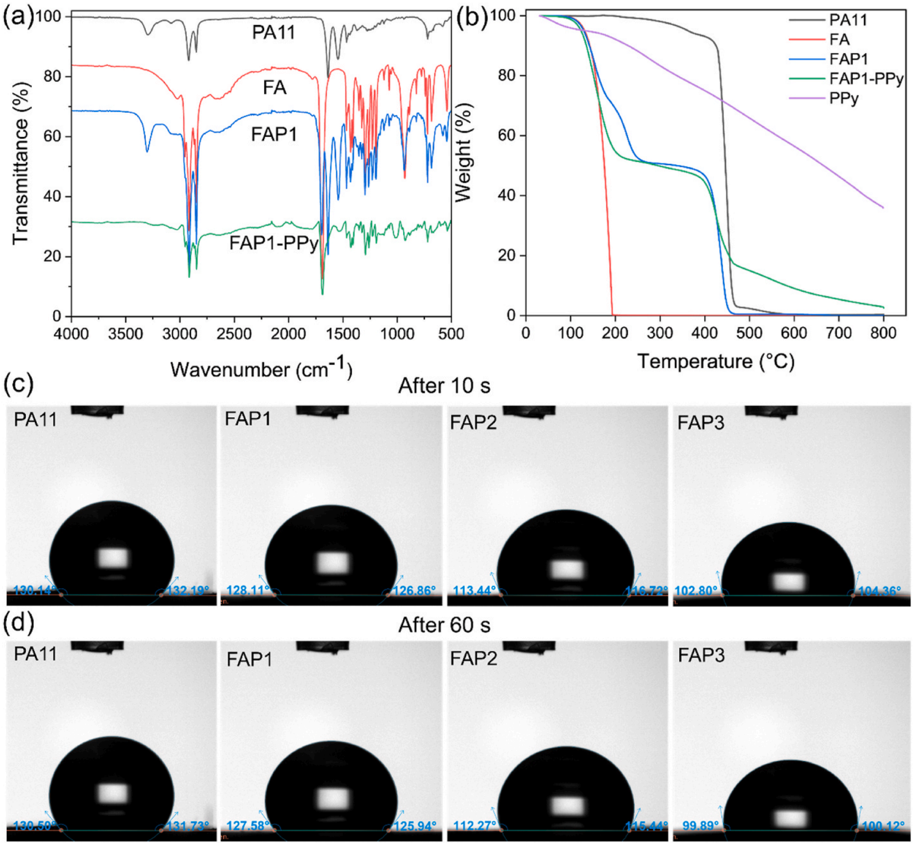

Fig. 2. a) FTIR spectra and b) TGA thermograms of the samples. The water contact angle for different samples c) 10 s and d) 60 s after deposition.

DSC 250 Auto. The sample was first equilibrated at −10 °C, then heated up to 60 °C with a heating rate of 5 °C/min, and finally cooled down to −10 °C. The heating-cooling cycles repeated three times under a nitrogen atmosphere. The phase change properties were extracted from the third cycle. The DA loading ratio (LR) in the fabrics was calculated by the following equation and compared with the experimental value.

$$LR(\%) = \frac{\Delta H_{mm} + \Delta H_{cm}}{\Delta H_{md} + \Delta H_{cd}} \times 100 \tag{1}$$

where ΔH_{mm}, ΔH_{cm}, ΔH_{md}, and ΔH_{cd} represent the melt and the crystallization enthalpy of the PCM fabrics and the melt and the crystallization enthalpy of neat DA, respectively. The phase change properties of the sample after the leak test were measured to investigate the stability of the developed PCM fibers. Besides, their cyclability was determined by subjecting the sample to 100 heating-cooling cycles. The thermal conductivity of the textile was measured using a TCi Thermal Conductivity Analyzer (C-Therm) that employed a modified transient plane source (MTPS) technique. A disk-shaped sample with a diameter of 15 mm was utilized for the measurement. The fabricated textile was exposed to light irradiation (studio 2000 OSRAM), and the temperature distribution was measured by thermal couples and recorded by a data acquisition system. The test was repeated while the textile was under a constant voltage.

3. Results and discussion

Fig. 1 represents the process of textiles fabrication as well as pyrrole *in-situ* polymerization on the textiles' surface schematically. PPy is a well-known H-bond donor [30]; hence, it can develop strong H-bonding with amine groups of PA11, as well as carboxyl groups of DA, leading to a stable conductive PPy layer on the DA/PA11 substrate as depicted in Fig. 1.

3.1. *Chemical composition and surface properties*

The FTIR spectra of PA11, DA, and the electrospun fabrics, i.e., FPA1, before and after coating are presented in Fig. 2a. The characteristic peaks of PA11 were similar to those reported for polyamides [31,32].

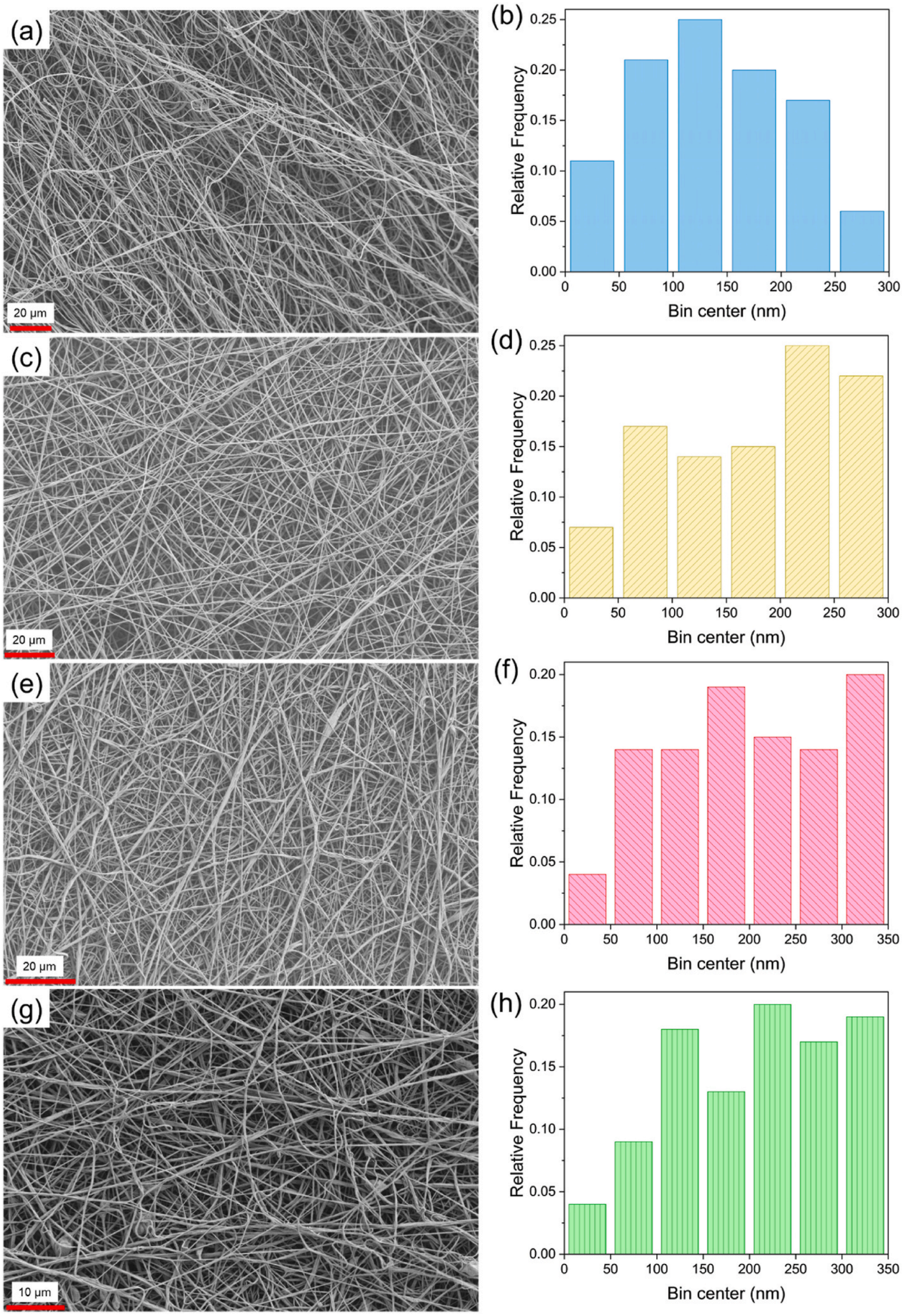

Fig. 3. SEM images and diameter distribution of a) and b) PA11, c) and d) FAP1, e) and f) FAP2, and g) and h) FAP3 fabrics.

Namely, a band at 3281 cm^{-1} was assigned to the hydrogen-bonded N–H stretching, the peaks at 2912^{-1} and 2851 cm^{-1} were attributed to asymmetric and symmetric stretching –CH vibrations of methylene groups, and the bands at 1631 cm^{-1} and 1545 cm^{-1} originated from stretching of the amide groups. Likewise, the characteristic peaks of DA matched those reported in the literature [33]. For instance, –CH$_3$ and –CH$_2$ symmetrical stretching vibrations appeared at 2915 cm^{-1} and 2855 cm^{-1}, C–O and C=O symmetrical stretching vibrations were revealed at 943 cm^{-1} and 1695 cm^{-1}, respectively, and the vibrations of –OH were obtained at 1430 cm^{-1}, 1305 cm^{-1}, and 724 cm^{-1}. PA11 and DA's characteristic peaks could be seen in the PCM fabric, i.e., FAP1, indicating the lack of any chemical reaction between the two components. The FTIR spectrum of the PPy-coated fabric, i.e., FPA1-PPy, significantly differed from the FAP1 one. The appeared peak agreed well with those reported for PPy [34]. For example, N–H contraction vibration appeared as a peak at 3421 cm^{-1}, the C=C stretching vibration of the pyrrole ring provided a band at 1545 cm^{-1}, the in-plane bending vibration of C–H on the ring resulted in a peak at 1025 cm^{-1}, and pyrrole ring vibration, =CH in-plane vibration, C–N stretching, and N–H in-plane absorption of the pyrrole ring originated characteristic peaks at 1542 cm^{-1}, 1433 cm^{-1}, 1122 cm^{-1}, and 1035 cm^{-1}, respectively [30]. Thus, FTIR confirmed that the deposited layer on the surface of FA1-PPy was a PPy layer.

TGA thermograms (Fig. 2b) were employed further to investigate the composition of the PCM and surface-coated fabrics and to study the PPy content qualitatively. The neat PA11 fabric presented a typical one-step thermal decomposition between 350 °C and 500 °C, with a maximum decomposition rate at 450 °C and an approximately zero residual weight percentage at 800 °C [31,32]. Likewise, DA revealed a typical one-step thermal decomposition behavior between 100 and 200 °C with a

Table 1
Electrical and mechanical properties of the electrospun fabrics.

Sample	Diameter (nm)	Conductivity (S/m)	Sheet resistance (S/Square)	Thermal conductivity (W/mK)	Tensile modulus (MPa)	Tensile strength (MPa)	Tensile strain (%)
	Before coating						
PA	140 ± 70	—[a]	—[a]	0.096 ± 0.006	56.72 ± 2.70	6.85 ± 0.29	114 ± 6
FAP1	180 ± 80	–	—[a]	0.075 ± 0.005	12.63 ± 0.61	4.11 ± 0.19	110 ± 6
FAP2	200 ± 85	–	—[a]	0.064 ± 0.005	10.75 ± 0.44	2.94 ± 0.12	73 ± 4
FAP3	210 ± 85	–	—[a]	0.067 ± 0.008	10.11 ± 0.51	2.6 ± 0.11	60 ± 3
	After coating						
PA-PPy	–	3.32 ± 0.17	230 ± 12	0.141 ± 0.05	62.36 ± 3.20	7.43 ± 0.41	114 ± 8
FAP1-PPy	–	14.44 ± 1.02	125 ± 9	0.252 ± 0.05	16.22 ± 0.75	4.54 ± 0.32	95 ± 5
FAP2-PPy	–	19.65 ± 0.88	95 ± 4.2	0.271 ± 0.07	15.42 ± 0.77	3.34 ± 0.15	60 ± 3
FAP3-PPy	–	28.89 ± 1.50	32 ± 1.7	0.288 ± 0.07	17.41 ± 0.95	2.67 ± 0.19	54 ± 3

[a] Out of the device measurement range.

maximum thermal decomposition peak at 190 °C and a residual weight percentage of approximately zero percent at 800 °C [35]. Both PA11 and DA decomposition stages could be seen in the PCM textile, i.e., FAP1, containing 50 wt% of each component. Besides, as expected, it showed approximately zero percent residual at 800 °C. The PPy-coated sample, i.e., FAP1-PPy, also presented a similar decomposition behavior, except that the residual weight percentage was approximately 2.63% at 800 °C. The difference between the residual weight of FAP1-PPy and the pristine FAP1, as well as pristine PPy at 800 °C, were used to determine the amount of deposited PPy [36]. The residual weight percentage of pristine FAP1 at 800 °C was approximately zero percent, while that of FAP1-PPy was 2.63%, and it was approximately 38.88% for pristine PPy. Thus, the PPy amount in the FAP1-PPy was calculated as 7.3%.

The wetting properties of the electrospun mats were examined by the water contact angle measurement. A droplet of water solution was placed on the sample surface, and the static contact angle was determined after 10 s (Figs. 2c) and 60 s (Fig. 2d). All samples presented a relatively hydrophobic surface with a water contact angle of over 100°, specifying a hydrophobic characteristic. The highest hydrophobicity was observed for the PA fabric, in which the contact angle was around 130°. The contact angle was almost the same after 60 s, indicating a stable surface characteristic [37]. In the PCM fabrics, the water contact angle decreased, whereas the sample with a higher DA loading showed the lowest contact angle. In other words, by increasing the fatty acid content, the hydrophobicity of the surface was altered, which could be due to the less hydrophobic property of DA compared to PA11. Thus, the PA11 surfaces could be readily controlled by using decanoic acid. The lower hydrophobicity in the PCM fabrics could be considered a positive property for PPy coating. As already explained, the pyrrole surface polymerization was designed in the current study to make the spun

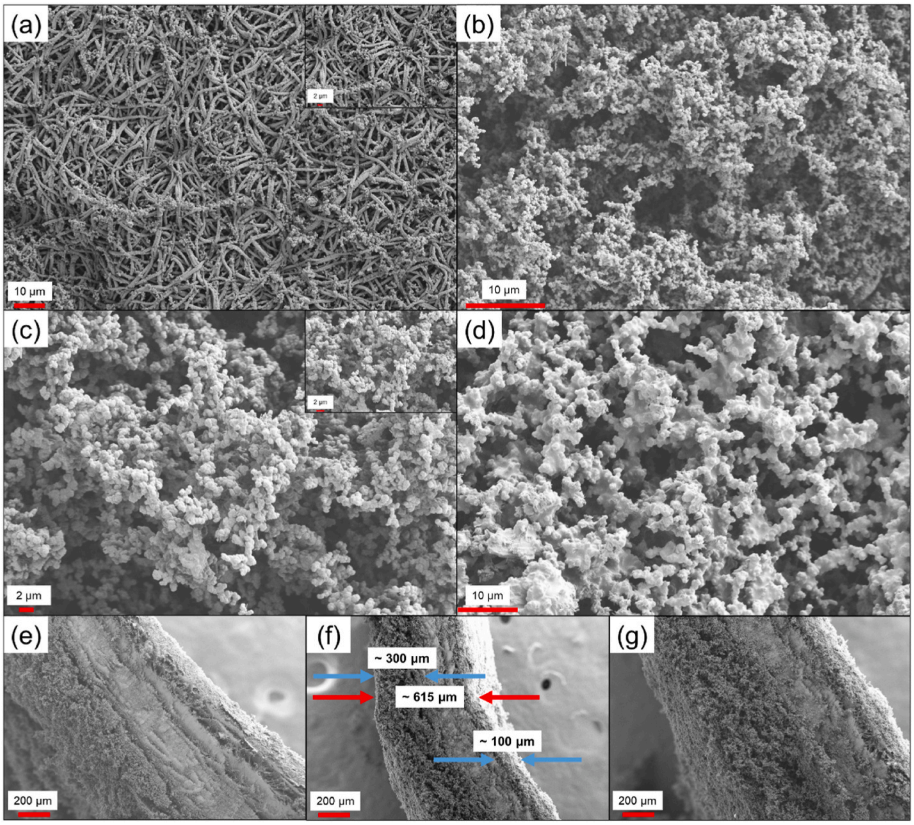

Fig. 4. SEM images a) PA11-PPy, b) FAP1-PPy, c) FAP2-PPy, and d) FAP3-PPy. SEM images from the cross-section area of e) FAP1-PPy, f) FAP2-PPy, and g) FAP3-PPy.

fabrics conductive. A more hydrophilic surface allowed better surface impregnation with pyrrole monomers, thereby achieving a better PPy coating with higher conductivity after polymerization, as will be discussed in the following sections. It is worth notifying that all PPy-coated PCM textiles presented highly hydrophilic surface properties, in which the water droplets adsorbed immediately after deposition. As Baig et al. [30] reported, it could be due to the formation of H-bonding between PPy and water molecules, which makes a super-hydrophilic surface after PPy surface polymerization.

3.2. Microstructure study

SEM imaging was employed to examine the morphology of the electrospun fabrics. The representative SEM images and diameter histogram of the produced nanofibers are given in Fig. 3. In all samples, structures were porous and highly homogeneous, with smooth, long, continuous, and free-bead fibers. Furthermore, the fibers' diameter was uniform along their length, without any evidence of fibers flatting. These observations indicated that the spinning parameters used in this experiment were suitable for preparing fibers in both neat PA and PCM textiles. Moreover, it could be seen that PCM fabrics exhibited well and stable nanofibrous network structure without any leakage of the DA, indicating that electrospun PA11 nanofibers could be acted as a kind of supporting material for decanoic acid PCM by capillary force adsorption and surface tension [38]. It is worth bearing in mind that in some research works that have been done on stabilizing fatty acid with polymer fibers, irregularly shaped defects, such as drops or mists, have been observed at a high loading of fatty acid attributed to the weakening of conjugations among polymer chains in the presence fatty acids, insufficient dispersion of fatty acids in polymer solutions, and the limited encapsulation capability of the selected polymer support [39]. However, in the current study, even at a very high DA loading of 70 wt %, i.e., FAP3 fabric, no apparent defect could be seen, proving the great potential of PA11 in stabilizing decanoic acid. The average diameter of the fibers is summarized in Table 1. The diameter increased from 140 ± 70 nm to 210 ± 85 nm over the addition of DA, which could be ascribed to the decreased charge density and surface tension, impeding the stretching of the jet yet, increasing the fibers' diameter [40,41]. It is worth noticing that we tried to spin the neat DA; however, we could not get high-quality bead-free fibers. In other words, the spinnability of the solution was due to the polyamide portion. When polyamide is mixed with a solvent, e.g., HFIP, its reactive functional groups may yield chemical exchange reactions. As a result, the solution shows a poly-electrolytic behavior. The applied strong electric field during electrospinning further drives the reactive ions in the polymer solution and forces them to come out from the needle tip. By relaxing the electrical stress aligned high-aspect ratio fibers are formed [42].

The morphology of the nanofibers after PPy surface polymerization was monitored by SEM images. The micrographs from the surface and cross-section of the PPy-coated textiles are presented in Fig. 4. A rough surface in which particles with nearly spherical morphology were uniformly distributed throughout the fibers could be seen in all samples, indicating the successful polymerization of pyrrole monomers [43]. Furthermore, no evidence of PPy agglomeration could be found, suggesting uniform growth of the PPy chains over the employed oxidative polymerization of pyrrole monomer. In all samples, especially the PCM textiles, all fibers were thoroughly covered by the polymeric mass of PPy, in which PPy particles were completely in contact with each other, a critical feature of having an electrically conductive surface. The higher the DA loading, the denser the PPy coating, which could be due to the higher surface wettability, as previously observed and discussed. Noticeably, the conductive fabrics still exhibited a well-developed porous structure, confirming that the in-situ polymerization did not cause the blocking of the pores of the mats.

SEM images taken from the cross-section area of the conductive PCM textiles, including FAP1-PPy, FAP2-PPy, and FAP3-PPy, were used to monitor the thickness of the coating layer. As provided in Fig. 4f, the thickness of the electrospun fabric (FAP2-PPy) was approximately 600 μm, roughly 400 μm of which was coated by the PPy particles. It means the pyrrole monomer penetrated to some extent into the inner layers of the spun fibers, and the polymerization was also done inside the fibrous structure. As can be seen, in the samples with a higher content of DA (Fig. 4g), more fibers were coated with PPy, which could be explained by the higher surface wettability at higher DA loadings.

3.3. Electrical and thermal conductivity

Due to alternating single-bond and double-bond in PPy's chemical structure as well as a conjugated polymer chain, PPy provides relatively high electrical conductivity. On the other hand, *in-situ* polymerization of PPy onto different structures has been reported as a feasible approach to fabricating PPy into various templates and creating a conductive surface [27,44]. The electrical conductivity (S/m) of the electrospun fibers before and after PPy coating as well as the sheet resistance values (S/Square) are summarized in Table 1. Before any treatment, i.e., surface polymerization, the fabrics were obviously electrically insulated. The in-situ polymerization resulted in the immobilization of PPy coating adhered to the polyamide/decanoic acid continuous fibrous network, and a continuous conducting pathway was formed, which enabled the fabrics to conduct electrons [45]. The conductivity enhanced with the increase in the DA contents, which could be due to the higher wettability of the surface, as previously observed and discussed. In other words, the PPy-coated fibers' shell became intact and thicker with a further increase in the DA portion; thus, contacts between conducting polymer regions remained less isolated from non-conducting regions and facilitated electrical conduction, resulting in a quick rise in conductivity [46]. The highest conductivity was 28.89 ± 1.50 S/m in the FAP3-PPy PCM textile, which was in the range of conductivity for conductive polymer as well as PPy-coated electrospun fabrics [47–49]. This indicated the stabilization of an excellent and compact PPy layer on the fibers' surface through the employed *in-situ* polymerization method.

Thermal conductivity plays a crucial role in efficiently converting solar energy into thermal energy. A high thermal conductivity ensures rapid heat transfer in PCM composites, thereby reducing the phase transition time [50]. In order to assess the thermal conductivity of the fabricated textiles, measurements were conducted, and the results are summarized in Table 1. The initial thermal conductivity of the textiles, prior to PPy coating, was relatively low. Specifically, the electrospun PA11 nanofibers exhibited a thermal conductivity of 0.096 ± 0.006 W/mK, significantly lower than the reported values for polyamides [51]. This lower thermal conductivity can be attributed to the porous structure of the spun mat, which hinders heat transfer within the sample. Furthermore, the PCM-integrated composites exhibited even lower thermal conductivity, likely due to the intrinsic lower thermal conductivity of decanoic acid compared to polyamide 11 [52].

Remarkably, all composite PCMs demonstrated a significant improvement in thermal conductivity after the application of PPy coating. For instance, the thermal conductivity of the FAP3 textile increased by approximately 330%, strongly confirming the beneficial effect of PPy coating on improving the substrate's thermal conductivity. The thermal conductivity showed a proportional increase with the DA content, which can be attributed to the higher electrical conductivity of textiles with greater DA loading, as previously observed and discussed. Importantly, the obtained results align with those reported for PPy-coated substrates [50,53], indicating the potential use of PPy-coated composites as thermal energy storage materials in practical applications [54].

3.4. Mechanical properties

The mechanical characteristic is one of the main parameters identifying the practical application of the newly developed materials.

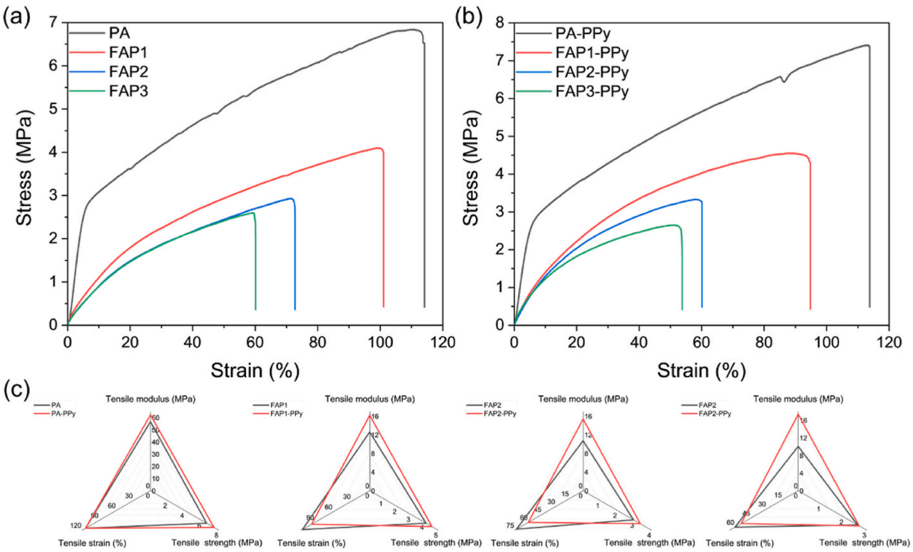

Fig. 5. Stress-strain curves of electrospun mats a) before and c) after coating with PPy. c) comparison of different mechanical properties of the electrospun mats before and after coating with PPy.

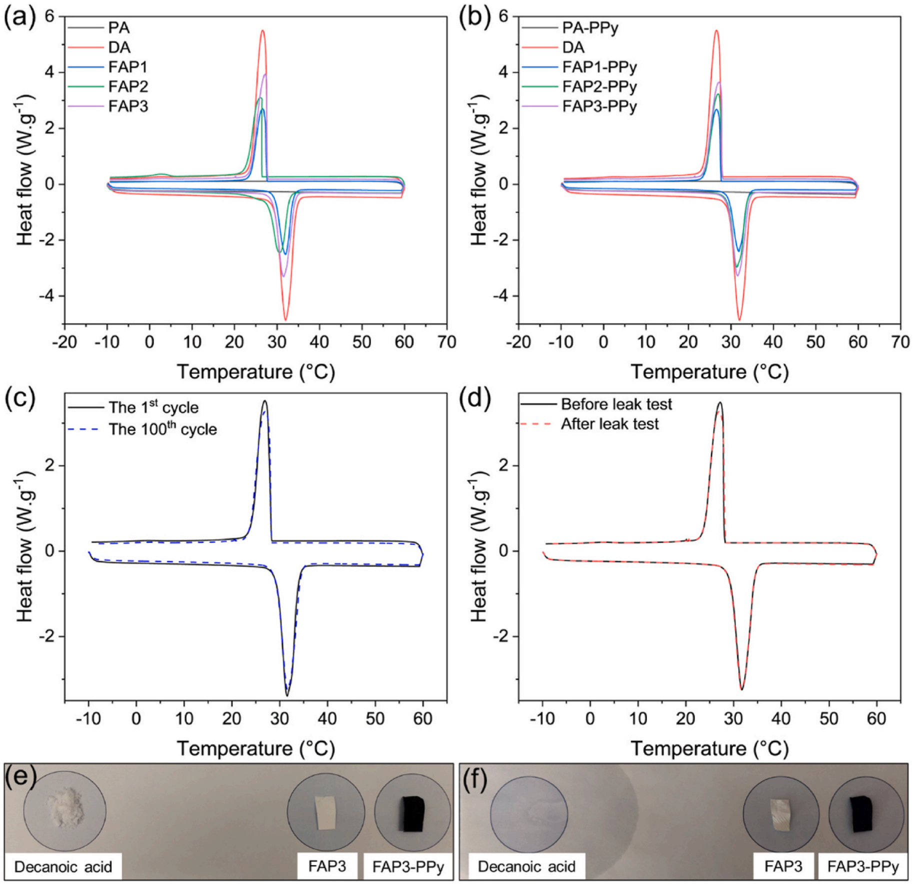

Fig. 6. DSC thermograms of neat DA and electrospun mats a) before and c) after PPy coating. c) the 1st and 100th DSC thermograms of FAP3-PPy. d) DSC DSC thermograms of FAP3-PPy before and after the leak test. e) and f) photograph of DA, FAP3, and FAP3-PPy before and after the leak test at 60 °C.

Therefore, the mechanical properties of the electrospun fabrics before and after surface coating were evaluated by tensile testing. The typical stress-strain curves and graphs comparing some important mechanical properties, i.e., tensile modulus, tensile strength, and tensile strain before and after surface coating, are illustrated in Fig. 5 and Table 1. The highest tensile modulus, tensile strength, and elongation at break were observed for the pristine PA11 fabric. All the above-mentioned mechanical properties decreased systematically upon the increase in the DA content. For instance, the tensile strength dropped from 56.72 ± 2.7 MPa in PA11 to 10.11 ± 0.51 in the FAP3 mat. The relatively high mechanical characteristics of plain PA11, previously reported by other researchers [55], may stem from the hydrogen bonding ability in the

Table 2
Phase change properties of the electrospun mats before and after PPy coating.

Sample	Onset (°C)	T_m (°C)	ΔH_m (J/g)	Onset (°C)	T_c (°C)	ΔH_c (J/g)	LR (%)
Before coating							
PA11[a]	–	–	–	–	–	–	–
DA	29.56	31.35	162.75	27.81	26.46	161.24	–
FAP1	28.93	30.57	80.25	27.55	27.19	79.81	49.4
FAP2	27.89	30.62	96.74	26.22	25.85	95.81	59.4
FAP3	28.58	31.05	112.77	28.58	26.65	110.21	68.8
After coating							
PA11-PPy	–	–	–	–	–	–	
FAP1-PPy	29.42	31.99	74.45	27.47	26.58	73.75	45.7
FAP2-PPy	29.44	31.41	89.35	27.96	26.97	88.68	54.9
FAP3-PPy	29.17	31.52	104.03	27.51	27.19	103.39	64.1
FAP3-PPy	29.17	31.52	103.95	27.51	27.19	103.21	64.1
FAP3-PPy	29.17	31.52	103.96	27.51	27.19	103.23	64.1

II Data are for the 100th cycle.
III The data are for after the leak test.
[a] PA11 did not show any phase change properties in the operating temperature range (−10 °C–60 °C).

PAs, resulting in better bonding between the layers of individual fibers. The dramatic reduction in mechanical performance could be justified by the poor mechanical properties of the plain DA as well as less hydrogen bonding density in the PCM fabrics. It could also be due to the lubricant/plasticizing effect of the fatty acid [56], as the tensile modulus also reduced considerably in the PCM textiles. The higher fibers' diameter in the PCM mats might be another reason for their noticeably lower mechanical performance [57]. It might be worth mentioning that the observed mechanical properties of the fabrics agreed well with the range reported for most electrospun polymer fabrics [47,58,59]. On the other side, as provided in Fig. 5, the mechanical properties slightly improved after the *in-situ* polymerization of pyrrole, which might be due to the hydrogen bonds of the PA11 and PPy [47,60]. As previously mentioned, conducting polymers like PPy have their shortcomings, such as fragility and rigidity, which lead to low mechanical strength after compounding with polymer substrate. Thus, our results strongly proved the benefit of pyrrole *in-situ* polymerization in developing conductive composites with significant mechanical properties.

3.5. Heat storage performance

In the practical applications of thermo-regulating textiles, the thermal properties generally play a crucial role. Thus, the heat storage capacity and the thermo-regulation property of the developed PCM textiles were measured using DSC. The melting-freezing process of PA11, FAP1, FAP2, and FAP3, as well as the neat DA, are illustrated in Fig. 6. Besides, the phase change properties, including onset temperatures, T_m, T_c, and phase change enthalpies, taken from DSC thermograms, are listed in Table 2. PA11 presented neither exothermic nor endothermic peaks, indicating that it had no phase change performance in the test temperature range. Unlike PA11, during the temperature change process, two prominent transition peaks were clearly observed in the DSC heating and cooling curves of pure DA, attributed to the destruction/formation of anisotropic lattices of crystalline decanoic acid multicores. In other words, DA underwent solid-liquid phase transitions in this temperature range, resulting in heat storage or heat release. The exothermic peak (crystallization peak) appeared at approximately 24.5 °C, while the endothermic one (melting peak) was around 31.5 °C. There was no obvious difference between the melting and solidification temperatures of neat DA and PCM textiles, indicating that the fabrics' crystallization process was not different from that of the pure DA. Moreover, the polyamide chains did not restrict the DA crystallization. However, the phase change enthalpies decreased proportionally to the DA contribution, specifying that the heat storage capacity of the developed phase change fibers was governed by a load of PCM in them. For example, the melting enthalpy reduced from 162.75 J/g in the neat DA to 80.25 J/g in the FAP1 containing 50 wt% DA. The phase change enthalpy values were used to calculate the loading ratio (LR) through **Equation (1)**. The calculated values are tabulated in Table 2. In all PCM mats, the calculated LR had good agreement with the experimental values, indicating the formation of the uniform solutions *via* mixing PA and DA as well as efficient loading of the DA into polyamides nanofibers. Likewise, the DSC curves, as well as the phase change properties of the samples after PPy surface polymerization, are presented in Fig. 6 and Table 2. After PPy coating, the phase change enthalpies reduced, obviously due to the reduction in the portion of phase change DA. According to the amount of coated PPy, i.e., 7.3%, previously calculated from TGA data, the LR values were slightly lower than expected, which might be due to incomplete crystallization of PCM in the fiber after PPy coating [61].

The thermal cycling was performed on the conductive textile with the highest DA content, i.e., FAP3-PPy, to examine the thermal cyclic (100 times) reliability of the produced conductive PCM textiles. The 1st and 100th cycles are presented in Fig. 6c. Furthermore, the whole 100 cycles are plotted in Fig. S1. Notably, no distinct changes were observed in the phase change temperatures and phase change enthalpies of FAP3-PPy after 100 cycles. For instance, both the melting and the crystallization enthalpy values after 100 times thermal cycles were almost equivalent to those of the first cycle within the measurement uncertainties (Table 2), indicating the favorable thermal storage stability of as-prepared nanofibrous mats, which is a must for long-term use as PCM [62,63].

The melting/crystallization processes take place when the temperature reaches the phase transition temperature of DA, and the molten DA may leak, restricting the practical application of the developed PCM

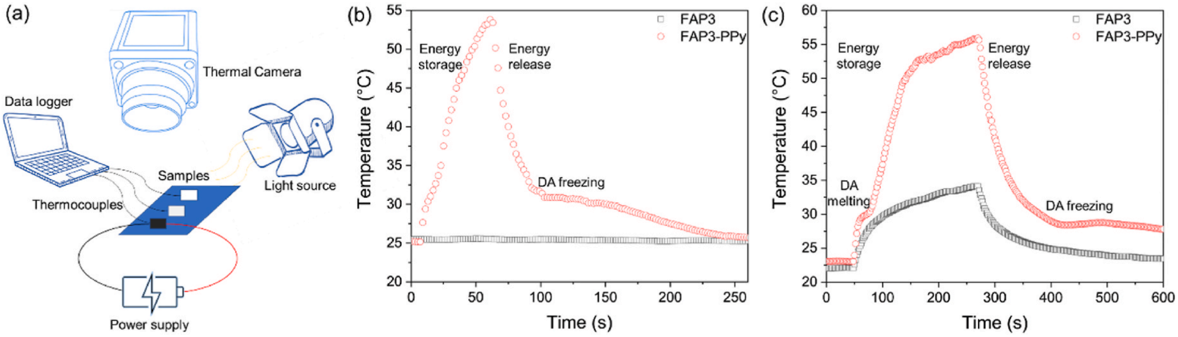

Fig. 7. a) Schematic illustration of the design setup for evaluation of the photo-/electro-thermal energy conversion and storage performance of the developed textiles. b) Temperature curves of the developed fabrics under b) voltage and c) light irradiation.

textiles. Therefore, the leakproof performance and shape stability of samples should be proved. The FAP3 and FAP3-PPy samples, as well as pure DA, were placed in a 60 °C oven to compare their leakage. The digital photos of the samples before and after the leak test are illustrated in Fig. 6e and f. As clearly seen, the pure DA completely melted, and the white bottom paper wetted, while no sign of paper wetting could be observed in the PCM textiles, indicating that the phase change process happened inside the nanofibers without any pronounced leakage. The leaked test sample, i.e., FPA3-PPy, was subjected to DSC measurement to calculate its phase change performance. The DSC graph is provided in Fig. 6d, and the relevant data are tabulated in Table 2. No obvious differences were seen in the phase change properties of the sample after the leak test, further proving the lack of DA leakage during the phase change process. To conclude, the DSC results proved that DA determined the heat storage capacity of the composite fabrics and performed its phase changes successfully. Moreover, the developed PCM fabrics had the property of heat storage and temperature regulation around 30 °C. Besides, the PCM textiles possessed excellent reliability, as well as leakproof performance. All in all, the developed PCM fibers are expected to provide valuable references for developing conductive thermoregulating textiles.

3.6. *Electro-/photo-thermal performance*

The electro-thermal and photo-thermal energy conversion/storage performance of the developed conductive textile, e.g., FAP3-PPy, were evaluated by applying voltage/light and monitoring the temperature using thermocouples on a setup design in our lab. The setup is schematically presented in Fig. 7a. The PCM fabric before surface coating with PPy, i.e., FAP3, was also tested for comparison. As already observed and discussed, PPy was uniformly deposited on the fabric, forming a continuous conductive path, which endowed the FAP3-PPy textile with good electrical conductivity. Thus, the FAP3-PPy textile was expected to respond rapidly to electrical stimuli; thereby, the electrical energy could be efficiently converted into thermal energy as Joule heat along the conductive path. As depicted in Fig. 7b, the FAP3 fabric did not show any pronounced temperature change under a constant voltage due to its insulated nature. However, in the conductive PCM textile, the temperature rose rapidly at the initial 60 s, suggesting a fast thermal response and high electro-thermal conversion rate. The maximum achieved temperature was approximately 55 °C, a higher temperature above the phase change temperature of DA. When the circuit was disconnected, the temperature of the FAP3-PPy textile dropped rapidly down to the phase change temperature of DA, i.e., 30 °C, demonstrating the fast heat dissipation of the fibers [9,64]. After that, a plateau area could be detected due to trapped DA's freezing. The temperature-time curve was followed by a gradual decrease in temperature, indicating that the FAP3-PPy textile was able to release the heat converted from electrical energy slowly [8]. In other words, in the phase change period, the electrical energy was stored in DA and subsequently released in the cooling process. The flattened part could not be seen on the ascending side of the chart, most probably due to the rapid increase in temperature after applying voltage. A similar trend was observed when the FAP3-PPy was exposed to light. As plotted in Fig. 7c, the temperature increased rapidly to 55 °C upon radiation. And it dropped when the light was turned off. Thus, one can conclude the high photo capture and fast heat dissipation among the fibers, thanks to the excellent photothermal conversion property of PPy [65]. The rate of temperature increase in the insulated textile, i.e., FAP3, was significantly lower than the conductive one. Furthermore, the maximum achieved temperature was lower, e.g., 35 °C. This result confirmed that the deposition of PPy coating on the textile considerably enhanced the light absorption and photo-thermal conversion performance of the substrate [53]. It is worth mentioning that the plateau area could be detected in both energy storage and energy release regions in the temperature-time curve, which was attributed to the DA's melting and freezing, respectively.

4. Conclusions

An electrospinning solution was developed in the current study to stabilize a relatively high amount of PCM decanoic acid in bio-based polyamide 11. Thus, up to 70 wt% of DA was loaded into the PA11 fibers without any obvious phase separation. The fabricated textiles provided a porous and highly homogeneous structure with smooth, long, continuous, and free-bead fibers. Furthermore, the diameter was uniform along their length, without any evidence of fibers flatting. The surface wettability improved upon increasing DA content, a positive characteristic of having higher electrical conductivity. Thus, a uniform and homogenous layer of PPy was polymerized on the surface of the developed textiles, resulting in electrical conductivity of up to 29 S/m. The tensile testing results confirmed the excellent mechanical performance and flexibility of the developed textiles, even after surface coating with a rigid layer of PPy. Besides, the conductive textiles revealed superb phase change properties with a latent heat of up to 113 J/g as well as outstanding thermal cycling reliability. It was also proved that the uniform PPy coating resulted in excellent electro-thermal and photo-thermal energy conversion and storage performance, making the developed flexible conductive PCM textiles exciting candidates in wearable and protective systems.

CRediT authorship contribution statement

Hossein Baniasadi: Writing – original draft, Visualization, Validation, Methodology, Investigation, Formal analysis, Conceptualization. **Despoina Chatzikosmidou:** Investigation. **Ari Kankkunen:** Investigation. **Jukka Seppälä:** Supervision, Funding acquisition. **Maryam R. Yazdani McCord:** Writing – review & editing, Visualization, Validation, Supervision, Resources, Project administration, Methodology, Investigation, Funding acquisition, Formal analysis, Conceptualization.

Declaration of competing interest

The authors declare that there is no conflict of interest.

Data availability

Data will be made available on request.

Acknowledgment

The authors would like to acknowledge financial support from Business Finland (7428/31/2022, PCMI project), the Research Council of Finland; No. 343192 (SoMa), No. 327248 (ValueBiomat), and No. 327865 (Bioeconomy). We thank Ari Seppälä for the thermal conductivity measurements.

Appendix A. Supplementary data

Supplementary data to this article can be found online at https://doi.org/10.1016/j.solmat.2023.112503.

References

[1] Y. Sha, W. Hua, H. Cao, X. Zhang, Properties and encapsulation forms of phase change material and various types of cold storage box for cold chain logistics: a review, J. Energy Storage 55 (2022), 105426.

[2] M.R. Yazdani, A. Laitinen, V. Helaakoski, L.K. Farnas, K. Kukko, K. Saari, V. Vuorinen, Efficient storage and recovery of waste heat by phase change material embedded within additively manufactured grid heat exchangers, Int. J. Heat Mass Tran. 181 (2021), 121846.

[3] M.R. Yazdani, A. Lagerström, V. Vuorinen, Simultaneous effect of biochar-additive and lightweight heat exchanger on phase change material for low-grade thermal energy storage, J. Energy Storage 55 (2022), 105478.

[4] C. Zhao, X. He, N. Sheng, C. Zhu, Directional fiber framework wrapped by graphene flakes for supporting phase change material with fast thermal energy storage properties, J. Energy Storage 57 (2023), 106304.

[5] H. Baniasadi, J. Seppälä, A. Kankkunen, A. Seppälä, M.R. Yazdani, Water-resistant gum-based phase change composite for thermo-regulating insulation packaging, J. Energy Storage 61 (2023), 106725.
[6] K. Turunen, M.R. Yazdani, A. Santasalo-Aarnio, A. Seppälä, Exceptional cold-crystallization kinetics of erythritol-polyelectrolyte enables long-term thermal energy storage, Sol. Energy Mater. Sol. Cells 230 (2021), 111273.
[7] E. Zdraveva, J. Fang, B. Mijovic, T. Lin, Electrospun poly (vinyl alcohol)/phase change material fibers: morphology, heat properties, and stability, Ind. Eng. Chem. Res. 54 (2015) 8706–8712.
[8] L. Chen, J. Lv, L. Ding, G. Yang, Z. Mao, B. Wang, X. Feng, S. Zapotoczny, X. Sui, A shape-stable phase change composite prepared from cellulose nanofiber/polypyrrole/polyethylene glycol for electric-thermal energy conversion and storage, Chem. Eng. J. 400 (2020), 125950.
[9] Z. Niu, S. Qi, S.S.A. Shuaib, W. Yuan, Flexible, stimuli-responsive and self-cleaning phase change fiber for thermal energy storage and smart textiles, Composites, Part B 228 (2022), 109431.
[10] K. Turunen, S. Li, M.R. Yazdani, Ionic mixture of binary sugar alcohols and a polymer: composition optimization for long-term thermal energy storage, ACS Sustain. Chem. Eng. 10 (2022) 15508–15519.
[11] R. Ji, Q. Zhang, F. Zhou, F. Xu, X. Wang, C. Huang, Y. Zhu, H. Zhang, L. Sun, Y. Xia, Electrospinning fabricated novel poly (ethylene glycol)/graphene oxide composite phase-change nano-fibers with good shape stability for thermal regulation, J. Energy Storage 40 (2021), 102687.
[12] H. Baniasadi, M. Madani, J. Seppälä, J.B. Zimmerman, M.R. Yazdani, Form-stable phase change electrospun nanofibers mat with thermal regulation and biomedical multi-functionalities, J. Energy Storage 68 (2023), 107660.
[13] Z. Niu, S. Qi, S.S.A. Shuaib, A. Züttel, W. Yuan, Flexible core-sheath thermochromic phase change fibers for temperature management and electrical/solar energy harvesting, Compos. Sci. Technol. 226 (2022), 109538.
[14] Y. Zhang, T. Li, S. Zhang, L. Jiang, J. Xia, J. Xie, K. Chen, L. Bao, J. Lei, J. Wang, Room-temperature, energy storage textile with multicore-sheath structure obtained via in-situ coaxial electrospinning, Chem. Eng. J. 436 (2022), 135226.
[15] X. Chai, T. Zhao, J. Yue, J. Yang, S. Zhang, J. Du, A. Zhang, Z. Feng, Flexible and degradable polycaprolactone based phase change composites for thermal energy management, React. Funct. Polym. 181 (2022), 105451.
[16] J. Wang, J. Xu, Y. He, Novel smart textile with ultraviolet shielding and thermo-regulation fabricated via electrospinning, J. Energy Storage 42 (2021), 103094.
[17] Y. Lu, X. Xiao, Y. Liu, J. Wang, S. Qi, C. Huan, H. Liu, Y. Zhu, G. Xu, Achieving multifunctional smart textile with long afterglow and thermo-regulation via coaxial electrospinning, J. Alloys Compd. 812 (2020), 152144.
[18] Y. Cai, C. Gao, X. Xu, Z. Fu, X. Fei, Y. Zhao, Q. Chen, X. Liu, Q. Wei, G. He, Electrospun ultrafine composite fibers consisting of lauric acid and polyamide 6 as form-stable phase change materials for storage and retrieval of solar thermal energy, Sol. Energy Mater. Sol. Cells 103 (2012) 53–61.
[19] C. Lin, W. Li, Y. Yan, H. Ke, Z. Liu, L. Deng, Z. Qiu, Ultrafine electrospun fiber based on ionic liquid/AlN/copolyamide composite as novel form-stable phase change material for thermal energy storage, Sol. Energy Mater. Sol. Cells 223 (2021), 110953.
[20] D. Li, Z. Pang, Q. Wang, H. Ke, Y. Cai, Y. Xu, F. Huang, Q. Wei, Fabrication and characterization of polyamide6-room temperature ionic liquid (PA6-RTIL) composite nanofibers by electrospinning, Fibers Polym. 14 (2013) 1614–1619.
[21] Y. Cai, X. Zong, J. Zhang, J. Du, Z. Dong, Q. Wei, Y. Zhao, Q. Chen, H. Fong, The improvement of thermal stability and conductivity via incorporation of carbon nanofibers into electrospun ultrafine composite fibers of lauric acid/polyamide 6 phase change materials for thermal energy storage, Int. J. Green Energy 11 (2014) 861–875.
[22] H. Chen, Q. Ma, S. Wang, H. Liu, K. Wang, Morphology, compatibility, physical and thermo-regulated properties of the electrospinning polyamide 6 and polyethylene glycol blended nanofibers, J. Ind. Text. 45 (2016) 1490–1503.
[23] R. Semnani Rahbar, H. Maleki, B. Kalantari, Fabrication of electrospun nanofibre yarn based on nylon 6/microencapsulated phase change materials, J. Exp. Nanosci. 11 (2016) 1402–1415.
[24] H. Baniasadi, J. Trifol, S. Lipponen, J. Seppälä, Sustainable composites of surface-modified cellulose with low–melting point polyamide, Mater. Today Chem. 22 (2021), 100590.
[25] H. Baniasadi, S. Lipponen, M. Asplund, J. Seppälä, High-concentration lignin biocomposites with low-melting point biopolyamide, Chem. Eng. J. 451 (2023), 138564, https://doi.org/10.1016/j.cej.2022.138564.
[26] H. Baniasadi, A. Ramazani S, A.S. Mashayekhan, M.R. Farani, F. Ghaderinezhad, M. Dabaghi, Design, fabrication, and characterization of novel porous conductive scaffolds for nerve tissue engineering, Int. J. Polym. Mater. Polym. Biomater. 64 (2015) 969–977.
[27] Y. Li, H. Yu, Y. Zhang, N. Zhou, Z. Tan, Kinetics and characterization of preparing conductive nanofibrous membrane by In-situ polymerization of Polypyrrole on electrospun nanofibers, Chem. Eng. J. 433 (2022), 133531.
[28] Y. Liang, X. Luo, Z. Hu, L. Yang, Y. Zhang, L. Zhu, M. Zhu, Deposition of ZIF-67 and polypyrrole on current collector knitted from carbon nanotube-wrapped polymer yarns as a high-performance electrode for flexible supercapacitors, J. Colloid Interface Sci. 631 (2023) 77–85.
[29] J. Wan, R. Hu, J. Li, S. Mi, J. Xian, Z. Xiao, Z. Liu, A. Mei, S. Xu, M. Fan, A universal construction of robust interface between 2D conductive polymer and cellulose for textile supercapacitor, Carbohydr. Polym. 284 (2022), 119230.
[30] U. Baig, A. Waheed, An efficient and simple strategy for fabricating a polypyrrole decorated ceramic-polymeric porous membrane for purification of a variety of oily wastewater streams, Environ. Res. 219 (2023), 114959.
[31] H. Baniasadi, S. Borandeh, J. Seppälä, High-performance and biobased polyamide/functionalized graphene oxide nanocomposites through in situ polymerization for engineering applications, Macromol. Mater. Eng. (2021), 2100255.
[32] H. Baniasadi, J. Seppälä, Novel long-chain aliphatic polyamide/surface-modified silicon dioxide nanocomposites: in-situ polymerization and properties, Mater. Today Chem. 20 (2021), https://doi.org/10.1016/j.mtchem.2021.100450.
[33] Y. Zhao, X. Lin, M. Hu, L. Xu, J. Ding, Y. Ding, Development and investigation of form-stable and cyclable decanoic acid-based composite phase change materials for efficient battery thermal management, J. Power Sources 558 (2023), 232615.
[34] N. Xiao, Investigation on corrosion inhibition performance of polypyrrole coating on Q235 steel in civil structure, Alex. Eng. J. 70 (2023) 547–551.
[35] Y. Konuklu, H.O. Paksoy, M. Unal, S. Konuklu, Microencapsulation of a fatty acid with Poly (melamine–urea–formaldehyde), Energy Convers. Manag. 80 (2014) 382–390.
[36] Y.S. Choi, S.H. Joo, S.-A. Lee, D.J. You, H. Kim, C. Pak, H. Chang, D. Seung, Surface selective polymerization of polypyrrole on ordered mesoporous carbon: enhancing interfacial conductivity for direct methanol fuel cell application, Macromolecules 39 (2006) 3275–3282.
[37] X. Zhang, J. Liu, H. Zhang, P. Wu, C. Liu, J. He, W. Jiang, Rapid separation of High-viscosity phosphorous Acid/Tributyl phosphate extraction system by a stable anticorrosive Super-PA-phobic mesh, Sep. Purif. Technol. 294 (2022), 121199.
[38] H. Ke, Q. Wei, Using co-electrospinning method to regulate phase change temperatures of fatty acid eutectic/polystyrene/fatty acid eutectic form-stable phase change composite nanofibrous membranes for thermal energy storage, Thermochim. Acta 683 (2020), 178438.
[39] W. Chen, W. Weng, Ultrafine lauric–myristic acid eutectic/poly (meta-phenylene isophthalamide) form-stable phase change fibers for thermal energy storage by electrospinning, Appl. Energy 173 (2016) 168–176.
[40] W. Zhou, J. Yu, S. Zhang, B. Ding, Direct electrospinning of fluorine-free waterproof polyamide/polydimethylsiloxane nanofibrous membranes with highly breathable performance, Compos. Commun. 35 (2022), 101337.
[41] Y. Xu, J. Wang, Z. Wang, Y. Zhao, W. Guo, Bio-based polyamide fibers prepared by mussel biomimetic modification of hydroxyapatite, Eur. Polym. J. 187 (2023), 111913.
[42] R. Nirmala, R. Navamathavan, H.-S. Kang, M.H. El-Newehy, H.Y. Kim, Preparation of polyamide-6/chitosan composite nanofibers by a single solvent system via electrospinning for biomedical applications, Colloids Surf. B Biointerfaces 83 (2011) 173–178.
[43] W. Matysiak, T. Tański, W. Smok, K. Gołombek, E. Schab-Balcerzak, Effect of conductive polymers on the optical properties of electrospun polyacrylonitryle nanofibers filled by polypyrrole, polythiophene and polyaniline, Appl. Surf. Sci. 509 (2020), 145068.
[44] B. Maharjan, V.K. Kaliannagounder, S.R. Jang, G.P. Awasthi, D.P. Bhattarai, G. Choukrani, C.H. Park, C.S. Kim, In-situ polymerized polypyrrole nanoparticles immobilized poly (ε-caprolactone) electrospun conductive scaffolds for bone tissue engineering, Mater. Sci. Eng. C. 114 (2020), 111056.
[45] D. Müller, C.R. Rambo, D.O.S. Recouvreux, L.M. Porto, G.M.O. Barra, Chemical in situ polymerization of polypyrrole on bacterial cellulose nanofibers, Synth. Met. 161 (2011) 106–111.
[46] I.S. Chronakis, S. Grapenson, A. Jakob, Conductive polypyrrole nanofibers via electrospinning: electrical and morphological properties, Polymer 47 (2006) 1597–1603.
[47] M. Zarei, A. Samimi, M. Khorram, M.M. Abdi, S.I. Golestaneh, Fabrication and characterization of conductive polypyrrole/chitosan/collagen electrospun nanofiber scaffold for tissue engineering application, Int. J. Biol. Macromol. 168 (2021) 175–186.
[48] T. Sudwilai, J.J. Ng, C. Boonkrai, N. Israsena, S. Chuangchote, P. Supaphol, Polypyrrole-coated electrospun poly (lactic acid) fibrous scaffold: effects of coating on electrical conductivity and neural cell growth, J. Biomater. Sci. Polym. Ed. 25 (2014) 1240–1252.
[49] E. Číková, M. Mičušík, A. Šišková, M. Procházka, P. Fedorko, M. Omastová, Conducting electrospun polycaprolactone/polypyrrole fibers, Synth. Met. 235 (2018) 80–88.
[50] X. Ye, L. Yang, Z. Tian, P. Zhou, S. Wang, H. Sun, Z. Zhu, J. Li, W. Liang, A. Li, Polypyrrole-coated conjugated microporous polymers/expanded graphene carbon aerogels based phase change materials composites for efficient energy conversion and storage, Sol. Energy Mater. Sol. Cells 245 (2022), 111873.
[51] W. Cao, M. Shaker, X. Meng, H. Feng, Large-scale fabrication of graphene/polyamide-6 composite as a high thermal conductivity engineering composite for thermal radiators, Mater. Lett. 316 (2022), 132036.
[52] Y. Li, H. Yan, Q. Wang, H. Wang, Y. Huang, Structure and thermal properties of decanoic acid/expanded graphite composite phase change materials, J. Therm. Anal. Calorim. 128 (2017) 1313–1326.
[53] Z. Tao, H. Zou, M. Li, S. Ren, J. Xu, J. Lin, M. Yang, Y. Feng, G. Wang, Polypyrrole coated carbon nanotube aerogel composite phase change materials with enhanced thermal conductivity, high solar-/electro-thermal energy conversion and storage, J. Colloid Interface Sci. 629 (2023) 632–643.
[54] Q. Chen, H. Wang, H. Gao, X. Wang, B. Ma, Effects of porous silicon carbide supports prepared from pyrolyzed precursors on the thermal conductivity and energy storage properties of paraffin-based composite phase change materials, J. Energy Storage 56 (2022), 106046.
[55] D. Li, W. Takarada, M. Ashizawa, T. Yamamoto, H. Matsumoto, Effect of hydrogen–deuterium exchange in amide linkages on properties of electrospun polyamide nanofibers, Polymer 229 (2021), 123994.
[56] M. Vlacha, A. Giannakas, P. Katapodis, H. Stamatis, A. Ladavos, N.-M. Barkoula, On the efficiency of oleic acid as plasticizer of chitosan/clay nanocomposites and

its role on thermo-mechanical, barrier and antimicrobial properties–Comparison with glycerol, Food Hydrocolloids 57 (2016) 10–19.

[57] R. Erdem, M. Ilhan, M.K. Ekmekci, Ö. Erdem, Electrospinning, preparation and photoluminescence properties of CoNb2O6: Dy3+ incorporated polyamide 6 composite fibers, Appl. Surf. Sci. 421 (2017) 240–246.

[58] S. Khataei, M.H. Al-Musawi, K. Asadi, S. Ramezani, M. Abbasian, M. Ghorbani, Effect of molecular weight and content of polyvinylpyrrolidone on cell proliferation, loading capacity and properties of electrospun green tea essential oil-incorporated polyamide-6/polyvinylpyrrolidone nanofibers, J. Drug Deliv. Sci. Technol. (2023), 104310.

[59] J.W. Yoon, Y. Park, J. Kim, C.H. Park, Multi-jet electrospinning of polystyrene/polyamide 6 blend: thermal and mechanical properties, Fash. Text. 4 (2017) 1–12.

[60] Q. Yan, B. Xin, Z. Chen, Y. Liu, Enhancement in photothermal conversion property of polypyrrole-decorated polyurethane/zirconium carbide fibrous membrane, Mater. Today Commun. 28 (2021), 102584.

[61] Z. Quan, Y. Xu, H. Rong, W. Yang, Y. Yang, G. Wei, D. Ji, X. Qin, Preparation of oil-in-water core-sheath nanofibers through emulsion electrospinning for phase change temperature regulation, Polymer 256 (2022), 125252.

[62] J. Zhang, Z. Mao, Z. Sun, D. Wang, A. Wei, Z. Xu, Q. Feng, Q. Wei, Preparation and characterization of structurally variable inorganic nanofibrous mats with large surface area for intelligent temperature regulation textiles, Colloids Surfaces A Physicochem. Eng. Asp. 658 (2023), 130633.

[63] N. Sarier, E. Onder, Thermal insulation capability of PEG-containing polyurethane foams, Thermochim. Acta 475 (2008) 15–21.

[64] B. Deng, L. Fang, K. Fang, X. Han, Y. Liang, Scalable preparation of MWCNTs/PAN conductive composite fibers with Tai Chi structure for thermotherapy textiles, Compos. Sci. Technol. 232 (2023), 109866.

[65] W. Fan, Y. Zhang, Y. Sun, S. Wang, C. Zhang, X. Yu, W. Wang, K. Dong, Durable antibacterial and temperature regulated core-spun yarns for textile health and comfort applications, Chem. Eng. J. 455 (2023), 140917.